Electric Power Systems Research 190 (2021) 106757

Contents lists available at ScienceDirect

Electric Power Systems Research

journal homepage: www.elsevier.com/locate/epsr

Controller hardware in the loop testing of microgrid secondary frequency control schemes

Siddhartha Nigam*, Olaoluwapo Ajala, Alejandro D. Domínguez-García, Peter W. Sauer

Department of Electrical and Computer Engineering, University of Illinois at Urbana-Champaign, Urbana, IL 61801, U.S.A.

ARTICLE INFO

Keywords:
Microgrid control
Centralized control
Distributed control
Controller hardware-in-the-loop

ABSTRACT

This paper describes a controller hardware-in-the loop (C-HIL) approach for testing centralized and distributed secondary frequency control schemes of AC microgrids operating in islanded mode. We describe the formulation of the secondary frequency control problem and the theory behind the centralized and distributed implementations of the control schemes. Then, we describe the testbed utilized for C-HIL testing activities. Finally, we provide the testing results that compare the performance (in terms of the system response time), and resilience (in terms of withstanding the failure of a control device), of both schemes.

1. Introduction

The past decade has seen a sharp rise in the deployment of distributed energy resources (DERs) in electric power grids across the globe [1]. Along with this continuing trend came the microgrid concept, which has been shown to be a promising approach for efficient integration and management of DERs [2–4]. Loosely speaking, a microgrid is a group of interconnected loads and DERs, within a small geographical footprint with clearly defined electrical boundaries, that act as a single controllable entity with respect to the external grid to which it is connected [5]. A microgrid can operate in both grid-connected and islanded modes. In islanded mode, frequency control is a major problem; this is due to the intermittent nature of renewable-based DERs, e.g., PV installations, and the utilization of power electronic inverters to interface DERs to the microgrid, which leads to low or no rotating inertia [6]. Among the various frequency control objectives, a key one is secondary frequency control [7], which entails ensuring that, following a change in operating point of the microgrid, the system-wide frequency returns to its nominal value.

Over the years, several coordination and control schemes for microgrid secondary frequency control have been proposed in the literature [8,9]. These schemes have primarily utilized centralized and decentralized decision-making approaches, which have several limitations. For example, the centralized decision-making approach is susceptible to a single point of failure, while the decentralized decision-making approach typically lacks the flexibility that is necessary for a seamless integration of additional resources. An alternative, the distributed decision-making approach, has gained some popularity among researchers in the last decade [10–13]. In theory, coordination and control schemes based on the distributed decision-making approach should overcome the limitations of its other counterparts. However, to the best of our knowledge, there is no study that quantifies and compares the performance of microgrid controls based on the distributed decision-making approach with those based on centralized or decentralized decision-making approaches, especially in the context of performing secondary frequency control. Hence, there is a need to test, validate, and compare the performance of these schemes so as to understand which one is best suited for microgrid frequency control.

Controller hardware-in-the Loop (C-HIL) testing is an effective way to test microgrid controls. In this paper, we describe such testing for two microgrid frequency control schemes. The first scheme is based on a centralized decision-making approach, while the second one is based on a distributed decision-making approach. The setup for testing the centralized control scheme comprises a National Instruments (NI) compact rio (cRIO) device, a centralized entity, that carries out secondary frequency control of an islanded AC microgrid whose components, i.e., the electrical network and its connected DERs and loads, are simulated using a Typhoon HIL real-time emulator (see [14], for details on a microgrid implementation using Typhoon HIL simulator). The setup for testing the distributed control scheme comprises the same emulated microgrid, but instead of using the NI cRIO device for centralized monitoring and control, several interconnected Arduino devices are used to implement our distributed algorithms for microgrid secondary frequency control (see [11,13,15], for details on these

* Corresponding author.
E-mail addresses: nigam4@illinois.edu (S. Nigam), ooajala2@illinois.edu (O. Ajala), aledan@illinois.edu (A.D. Domínguez-García), psauer@illinois.edu (P.W. Sauer).

https://doi.org/10.1016/j.epsr.2020.106757
Received 4 October 2019; Received in revised form 10 April 2020; Accepted 2 August 2020
Available online 24 August 2020
0378-7796/

algorithms). Each Arduino device utilizes the information acquired, e.g., from measurements and other information obtained through exchanges with other nearby arduino devices, to perform successive computations and adjust the set-points of each controllable entity in the emulated microgrid, so as to achieve the secondary frequency control objective. We provide experimental results obtained from the C-HIL testing of both schemes, and utilize well defined metrics, e.g., the system response time and system resilience to a control device failure, to qualitatively and quantitatively compare them.

The remainder of this paper is organized as follows. In Section 2, we describe the secondary frequency control problem for an islanded AC microgrid with inverter-interfaced DERs. In Section 3, we provide a description of the C-HIL setup for testing the centralized and distributed coordination and control schemes. In Section 4, we present the C-HIL testing results for the two aforementioned frequency control schemes and compare their performance. Finally, in Section 5, we provide concluding remarks.

2. Secondary frequency control of islanded AC microgrids

In this section, we first describe the microgrid model adopted in this work, and provide an overview of the frequency control problem (see [15] for details). Afterwards, we describe two schemes that solve the secondary frequency control problem; one of them is based on a centralized decision-making approach, whereas the other one is based on a distributed decision-making approach.

2.1. Microgrid model and the frequency control problem

The secondary frequency control schemes are tested on a real-time simulation of a three-phase microgrid whose mathematical model is based on the following assumptions:

A1. the phases are balanced,
A2. the transmission lines comprising the electrical network are short and lossless,
A3. the DERs and loads are interfaced via voltage-source inverters,
A4. the frequency and voltage magnitude of each inverter are controlled using the droop control laws described in [12,16,17],
A5. all the quantities are in per-unit, and the voltage reference values of each DER and/or load serves as its base voltage,
A6. the dynamics of the network, the inverter's filter, and the outer voltage controller comprise the fastest dynamic phenomena in the system,
A7. the dynamics of the voltage droop control are much faster than those of the frequency droop control,
A8. the dynamics of the outer voltage controller and inner current controller are much faster than those of the droop control, and
A9. the inverter reactive power capability is sufficient to support voltage control.

Accordingly, for each bus $i \in \mathcal{V}_p^{(g)}$: $=\{1, 2, ..., m\}$ that a DER is connected to, we have that

$$\begin{aligned} D_i \frac{d\theta_i(t)}{dt} &= u_i(t) - \sum_{j \in \mathcal{N}_p(i)} B_{ij} \sin(\theta_i(t) - \theta_j(t)), \\ \underline{u}_i &\le u_i(t) \le \overline{u}_i, \end{aligned} \tag{1}$$

where $\mathcal{N}_p(i)$ is the set of buses to which bus i is electrically connected, $\theta_i(t)$ is the bus voltage phase angle relative to a reference frame that rotates at some nominal frequency, e.g., 60 Hz, $u_i(t)$ is the active power set-point, $\underline{u}_i$ and $\overline{u}_i$ are lower and upper limits for the set-point, respectively, D_i is the droop coefficient for frequency control, and B_{ij} is the absolute value of susceptance for the line that connects buses i and j. Similarly, for each bus $i \in \mathcal{V}_p^{(\ell)}$: $=\{m+1, m+2, ..., n\}$ that a load is connected to, we have that

$$D_i \frac{d\theta_i(t)}{dt} = -(\ell_i^0 + \Delta\ell_i(t)) - \sum_{j \in \mathcal{N}_p(i)} B_{ij} \sin(\theta_i(t) - \theta_j(t)), \tag{2}$$

where ℓ_i^0 is the nominal active power demand and $\Delta\ell_i(t)$ is the active power demand perturbation. For the microgrid whose dynamics are described by (1) and (2), the following control objectives must be satisfied [15]:

O1: For ℓ_i^0, $i \in \mathcal{V}_p^{(\ell)}$, find, u_i^*, $i \in \mathcal{V}_p^{(g)}$, such that:
- $\sum_{i \in \mathcal{V}_p^{(g)}} u_i^* = \sum_{i \in \mathcal{V}_p^{(\ell)}} \ell_i^0$, $\quad \underline{u}_i \le u_i(t) \le \overline{u}_i$, and
- for $i \in \mathcal{V}_p^{(g)} \cup \mathcal{V}_p^{(\ell)}$, there is an equilibrium point θ_i^* that satisfies the phase cohesive condition described in [18].

O2: For sufficiently small changes in $\Delta\ell_i(t)$, $i \in \mathcal{V}_p^{(\ell)}$, regulate the value of each $u_i(t)$, $i \in \mathcal{V}_p^{(g)}$, around u_i^* such that
- $\frac{d\bar{\theta}_i(t)}{dt} \to 0$ as $t \to 0$.

A complete frequency regulation scheme requires achieving control objectives **O1** and **O2**. However, the scope of this paper focuses on the secondary frequency control problem, which pertains to objective **O2**. Here, we assume that, given each ℓ_i^0, $i \in \mathcal{V}_p^{(\ell)}$, the values of u_i^*, $i \in \mathcal{V}_p^{(g)}$, that satisfy the requirements of objective **O1** have been computed. Following any load perturbations, the secondary frequency control problem requires the active power set-points, $u_i(t)$, $i \in \mathcal{V}_p^{(g)}$, to be adjusted around the u_i^*'s via a closed-loop control feedback so as to eliminate the mismatch between total generation and total load. After several load perturbations or a large load change, it is necessary to recompute the u_i^*'s so as to meet objective **O1** (see [15], for details).

We define the average frequency error (AFE) at $t \ge 0$ as follows:

$$\Delta\bar{\omega}(t) := \frac{\sum_{i=1}^n D_i \frac{d\bar{\theta}_i(t)}{dt}}{\sum_{i=1}^n D_i}, \tag{3}$$

which, after substituting in (1) and (2), simplifies to:

$$\Delta\bar{\omega}(t) = \frac{1}{\sum_{i=1}^n D_i} \left(\sum_{i \in \mathcal{V}_p^{(g)}} u_i(t) - \sum_{i \in \mathcal{V}_p^{(\ell)}} (\ell_i^0 + \Delta\ell_i(t)) \right). \tag{4}$$

We now make use of the AFE expression in (4) to describe the centralized and distributed secondary frequency control schemes that were tested and compared in this work.

2.2. Centralized secondary frequency control scheme

This scheme requires a centralized control node that can communicate bidirectionally with DERs and loads in the microgrid so as to gather local information from each asset and instruct the DERs to change their active power set-points as needed—we assume that the loads are not controllable, as a result, a unidirectional communication link from the loads to the control node is sufficient. Fig. 1(a) depicts a six-bus microgrid with a centralized control node. In this case, using (4), the centralized control node can easily compute the AFE if it has access to the power injections at the buses the DERs and loads are connected to. Then, as proposed in [15], once the AFE is computed, its value is fed to a proportional-integral control that gradually drives the value of the AFE to zero by adjusting the value of each set-point $u_i(t)$, $i \in \mathcal{V}_p^{(g)}$.

In order to implement the centralized secondary frequency control scheme, the time is discretized into rounds $r = 0, 1, 2...$, with each having a fixed time duration T_0. Let

$$u_i[r] := u_i(t), \quad t_r \le t < t_{r+1},$$

where t_r denotes the beginning of round r, and $t_{r+1} - t_r = T_0$. Then, (4) can be written as:

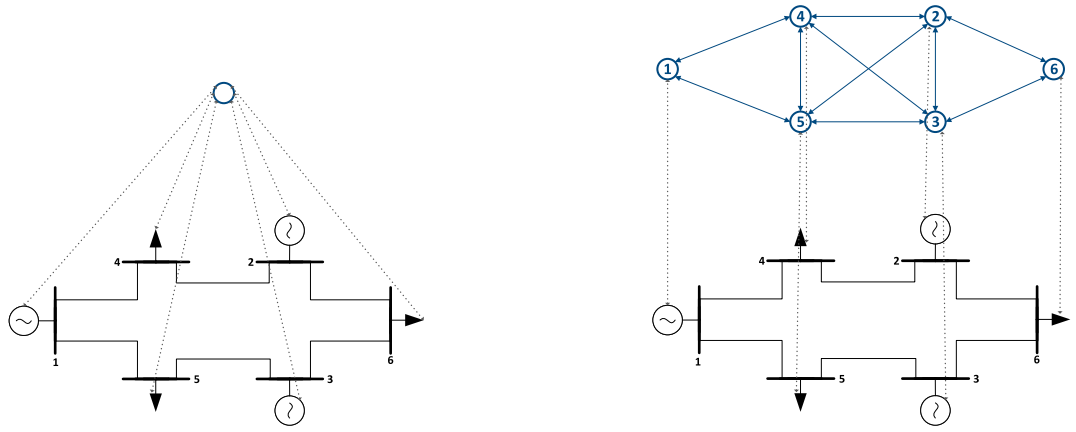

(a) A centralized control node connected to three DERs and three controllable loads.

(b) Six (distributed) control nodes interconnected via a communication network. Each control node is connected to a DER or controllable load.

Fig. 1. A schematic showing centralized and distributed control nodes connected to a six-bus islanded AC microgrid.

$$\Delta\overline{\omega}[r] = \overline{D}\left(\sum_{i\in\mathcal{V}_p^{(g)}} u_i[r] - \sum_{i\in\mathcal{V}_p^{(\ell)}} (\ell_i^0 + \Delta\ell_i)\right), \tag{5}$$

where $\overline{D} := \frac{1}{\sum_{l=1}^{n} D_l}$. As a result, the active power set-point of generator $i \in \mathcal{V}_p^{(g)}$ is adjusted according to:

$$e_i[r+1] = e_i[r] + \kappa_i \Delta\overline{\omega}[r], \tag{6}$$

$$u_i[r] = u_i^* + \alpha_i e_i[r], \tag{7}$$

where $e_i[0] = 0$, and α_i and κ_i are appropriately chosen gains (see [15] for details).

2.3. Distributed secondary frequency control scheme

In this scheme, each DER will also adjust its active power set-point according to (6) and (7). However, in order to do so, the DERs obtain the gains α_i and κ_i in a distributed manner, and compute the AFE, $\Delta\overline{\omega}[r]$, in a distributed fashion. To this end, the microgrid is endowed with multiple, geographically dispersed, computing devices referred to as distributed control nodes.

Fig. 1(b) provides a depiction of six distributed control nodes, each connected to a DER or load, in a six-bus microgrid. Each distributed control node can acquire information locally, e.g., control node 1 has access to the power injected by the DER connected to bus 1. In addition, the control nodes can exchange information among themselves; this is captured by the undirected communication graph in Fig. 1(b). For example, control node 6 can exchange information with control nodes 2 and 3, and they are referred to as the neighbors of control node 6 (i.e., the neighbors of a particular control node are the control nodes with which this particular node can directly exchange information with). The control nodes use the information they acquire locally, e.g., from measurements, and via exchanges with their neighbors, as inputs to the so-called ratio consensus algorithm (see, e.g., [10], [13], [15]). Through the ratio-consensus algorithm, each control node computes the AFE in a distributed manner. The computed AFE is used by the control nodes to adjust the active power set-points of the DERs according to (6) and (7).

2.3.1. The ratio consensus algorithm

The neighbors of control node i, i.e., the control nodes that node i communicates with bidirectionally, are represented by the set $\mathcal{N}_c(i)$. Each control node i maintains two internal states, y_i and z_i, which, at iteration k, it updates as:

$$y_i[k+1] = \sum_{j\in\mathcal{N}_c(i)\cup\{i\}} \frac{1}{|\mathcal{N}_c(j)|+1} y_j[k], \tag{8}$$

$$z_i[k+1] = \sum_{j\in\mathcal{N}_c(i)\cup\{i\}} \frac{1}{|\mathcal{N}_c(j)|+1} z_j[k]. \tag{9}$$

Right before each iteration, node i broadcasts its states to its neighbors and after iteration k, they are used to compute $\gamma_i[k] = \frac{y_i[k]}{z_i[k]}$. This is repeated until a finite number of iterations, K, is reached when $\gamma_i[K]$ is close to $\frac{\sum_i y_i[0]}{\sum_i z_i[0]}$ for all i—the value of K can be determined as described in [19].

In order to implement the distributed secondary frequency control scheme, define

$$x_i[r] = \begin{cases} u_i[r], & i \in \mathcal{V}_p^{(g)}, \\ -(\ell_i^0 + \Delta\ell_i), & i \in \mathcal{V}_p^{(\ell)}, \end{cases} \tag{10}$$

then $\Delta\overline{\omega}[r] = \frac{\sum_{i\in\mathcal{V}_p} x_i[r]}{\sum_{i\in\mathcal{V}_p} D_i}$. Accordingly, $y_i[0] = x_i[r]$ and $z_i[0] = D_i$ for each round r, and we have that, for each control node i,

$$\lim_{k\to\infty} \frac{y_i[k]}{z_i[k]} = \Delta\overline{\omega}[r].$$

Thus, using the ratio-consensus algorithm at each round r, each distributed control node can learn the value of $\Delta\overline{\omega}[r]$ and as a result, use that information to adjust the active power set-points of the DERs according to (6) and (7). While the ratio consensus formulation described here is not robust against communication packet drops and is for the case where each communication link between the control nodes is bidirectional, the variant of the ratio-consensus algorithm that is implemented in the C-HIL testbed is robust against packet drops and it supports unidirectional communication links (see [20], for details).

2.3.2. A failure-adaptive ratio consensus

In order to make the distributed scheme adaptive to failures of distributed control nodes, we developed a protocol that ensures that each node's contribution to the ratio consensus result can be taken up by its neighbors when the node fails. We assume that when a distributed control node fails, the DER or load it is connected to remains operational without changing its set-point, and the goal is that the value of this set-point is taken into account during the ratio consensus computations.

This failure-adaptive variant of ratio-consensus is implemented by first ensuring that during the first iteration of each ratio-consensus round, all control nodes store the data received from their neighbors. At

the same time, each distributed control node also randomly selects from its neighbors an *inheritor*, and each inheritor is notified of its status. The data received from node i during the first iteration is $\frac{y_i[0]}{\delta_i+1}$ and $\frac{z_i[0]}{\delta_i+1}$, where $\delta_i = |\mathcal{N}_c(i)|$ represents the number of neighbors of node i. When node i fails, each neighbor j of node i, except the *inheritor*, adjusts its initial values to $y_j[0] + \frac{y_i[0]}{\delta_i+1}$ and $z_j[0] + \frac{z_i[0]}{\delta_i+1}$. At the same time, $\frac{2y_i[0]}{\delta_i+1}$ and $\frac{2z_i[0]}{\delta_i+1}$ are added to the initial conditions of the inheritor, $y_j[0]$ and $z_j[0]$, respectively. Accordingly, when node i fails, the sum of initial conditions of control nodes $j \in \mathcal{N}_c(i)$ becomes

$$\sum_{j\in\mathcal{N}_c(i)} y_j[0] + y_i[0] \qquad \text{and} \qquad \sum_{j\in\mathcal{N}_c(i)} z_j[0] + z_i[0],$$

respectively, and the initial condition of the distributed control node that failed is preserved. This protocol ensures that during implementation of the distributed secondary frequency control scheme, the ratio consensus result is resilient to the failure of a control node.

3. C-HIL testing of centralized and distributed frequency control schemes

In this section, we describe two C-HIL testbed setups, one for testing the centralized frequency control scheme, and the other for testing the distributed control scheme. The C-HIL testbed is comprised of two layers, the physical layer and the cyber layer. In both setups, the physical layer comprises a real-time emulation of an islanded AC microgrid network and the loads and DERs connected to it. In the centralized setting, the cyber layer comprises a single control node on which the centralized control scheme is implemented, and in the distributed setup, the cyber layer comprises several control nodes implementing the distributed algorithms used for implementation of the distributed frequency control scheme. More details on the C-HIL testbed and its capabilities are provided in [21].

3.1. Physical layer

The physical layer comprises a Typhoon HIL real-time emulator that is used to simulate the microgrid electrical power network and the DERs and loads connected to it. The Typhoon HIL hardware provides simulation step sizes as low as 0.5 μs that allows us to test various control schemes in a high-fidelity setting. Specific details on the role of the Typhoon hardware in our C-HIL testbed are provided in [21]. The microgrid, the model of which is described by (1) and (2), is emulated on a Typhoon HIL device. The microgrid electrical network, shown in Fig. 1, consists of six buses with three buses connected to inverter-interfaced DERs and three buses connected to inverter-interfaced loads. The test system specifications are provided in [15].

3.2. Centralized scheme testing

To implement the centralized frequency control scheme on a C-HIL testbed, we made use of the National Instruments (NI) CompactRIO (c-RIO) 9068, which is an industrial grade real-time microcontroller. The cRIO provides an easy way to implement the control scheme using the NI Labview system design software. The cRIO controller also provides the capabilities to implement modbus TCP/IP protocol which allows us to interface the controller with the Typhoon HIL device.

In Fig. 2(a), we provide a depiction of the C-HIL testbed setup for testing the centralized frequency control scheme. The cRIO collects the power injection measurements from each DER/load in the emulated microgrid, uses them to calculate the AFE, and then uses (6) and (7) to compute new set-points for each DER in the microgrid. To close the control loop, the cRIO sends these new set-points to the DERs modeled in Typhoon HIL.

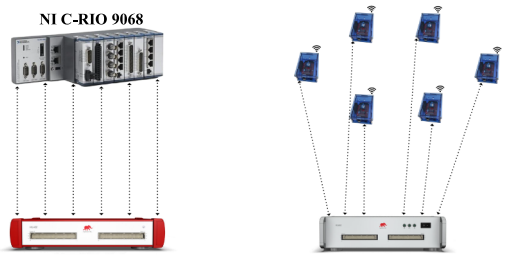

(a) C-HIL testbed setup for centralized control. (b) C-HIL testbed setup for distributed control.

Fig. 2. C-HIL testbed setup for testing centralized and distributed control schemes.

3.3. Distributed scheme testing

To monitor and control DERs and loads in the emulated microgrid, in a distributed fashion, six Arduino Due microcontrollers serve as the distributed control nodes. Each device is interfaced with an ethernet shield. This allows the control nodes to communicate with the Typhoon HIL device via the Modbus TCP/IP protocol so as to enable monitoring and control of DERs and loads in the emulated microgrid. In addition, each control node also has a MaxStream XB24-DMCIT-250 revB XBee wireless module which allows the control nodes communicate and exchange information with their neighbors.

Each control node implements the ratio consensus algorithm, and this enables a distributed computation of the AFE. The pertinent distributed control nodes utilize the AFE to compute new set-points for DERs in the emulated microgrid that they are connected to. The speed at which the distributed scheme computes the AFE depends on how fast the ratio consensus algorithm converges., and the rate of convergence heavily depends on the connectivity of the communication network. For example, for the case where each distributed control node is directly connected to every other control node in the system, the convergence speed is the same as that achieved with the centralized scheme. Fig. 2(b) depicts the communication network topology that was implemented in our C-HIL testbed, as well as the communication links between the control nodes and the DERs or loads.

4. C-HIL testing results

We start out by describing the active power profiles that were used for testing both schemes. Afterwards, we present results depicting the load change, the system frequency response, and the DER set-point changes. For comparison, we make use of two performance objectives, namely, response time and resilience, both of which highlight the effects of each secondary frequency control scheme.

4.1. Active power profiles of DERs and loads

For the six bus islanded AC microgrid considered, the total power initially demanded by the loads is taken to be 3.3 pu with individual loading $\ell_i^0 = 1.15$ pu, 1.25 pu, and 0.9 pu respectively for $i = 4$, 5, 6. At time $t = 0^-$, prior to the start of the test, the DER set-points corresponding to the microgrid equilibrium points, θ_i^*, $i = 1, \cdots, 6$, are $u_i^* = 0.85$ pu, 1.5 pu, and 0.95 pu respectively for $i = 1$, 2, 3. The frequency control droop coefficients are: $D_1 = 0.225$, $D_2 = 0.679$, $D_3 = 0.95$, $D_4 = 0.0125$, $D_5 = 0.0679$, and $D_6 = 0.0479$. We ran a 150 second long C-HIL real-time simulation with the following perturbations to the system:

(i) At the 30 second mark, the load ℓ_6 changes to 1.4 pu from 0.9 pu (see Fig. 3).
(ii) At the 60 second mark, the microgrid loses DER u_1 from the network (see Figs. 5(a), 5(b), 7(a), and 7(b)).

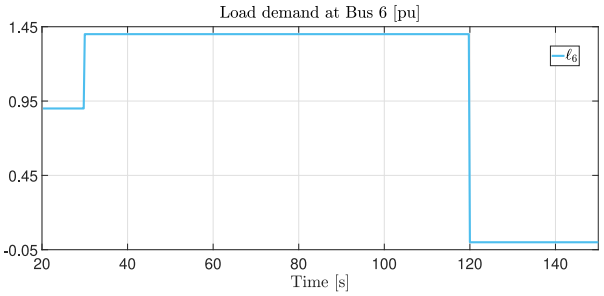

Fig. 3. Varying load demand at Bus 6.

(iii) At the 120 second mark the microgrid loses load ℓ_6 (see Fig. 3).

4.2. Response time

This performance objective entails identifying which frequency control scheme, centralized or distributed, is faster in terms of restoring the system frequency to its nominal value. The perturbations described in Section 4.1 were applied to the system and the performance of both control schemes were recorded. We present results depicting the frequency response and the DER set-point changes associated with each control scheme.

Focusing on the period between 20 s and 150 s, Fig. 4 presents the frequency response of each bus as the load changes and as the microgrid loses a DER and a load. For the same profile, in Fig. 5, we provide the adjusted DER set-points. As the load ℓ_6 increases at 30 s, the frequency falls below 60 Hz, and both the centralized and distributed control schemes bring it back to the nominal value, as shown in Fig. 4. In Fig. 5, we see the adjusted set-points of the 3 DERs. At 60 s, the microgrid loses the DER connected to bus 1 (see Fig. 1), and both schemes fix the frequency error with the remaining 2 DERs compensating for the loss of generation. At 120 s, the microgrid loses the load ℓ_6 and both schemes fix the frequency error with the remaining 2 DERs reducing their generation set-points appropriately.

The results in Fig. 4 show that the response time of the centralized scheme to eliminate the frequency error due to any perturbations is shorter than that of the distributed scheme. The centralized scheme corrects the frequency error on each bus under any perturbation within 2 s, while the distributed scheme takes around 12 s to bring the frequency value back to the nominal value of 60 Hz. Since the centralized controller has direct access to information on the set-points and active power injections of the DERs and loads, it can compute the AFE and eliminate the frequency error as soon as there is a perturbation. The increased time in the distributed scheme is due to the computational time incurred by the ratio-consensus algorithm.

4.3. Resilience

This performance objective entails identifying which secondary frequency control scheme, centralized or distributed, is more resilient. We implemented the same DER/load power profile described in 4.1 but added some additional events. For testing the resilience of the centralized control scheme to a failure of the control node, we unplugged the c-RIO device at the 80 s mark so as to mimic its failure. For the distributed scheme, we unplugged two control nodes at times 80 s and 100 s, respectively. Next, we present results depicting the frequency response and the DER set-point changes associated with each control scheme after the aforementioned failures.

As the load ℓ_6 increases at the 30 s mark and as the microgrid loses the generation at 60 s mark, both centralized as well as distributed schemes are able to regulate the frequency and bring it back to 60 Hz. The difference in performance between the two schemes starts to show after we take out the centralized controller in the centralized scheme and the control nodes 1 and 4 in the distributed scheme. The frequency is nominal as the centralized controller is unplugged in the centralized scheme. As the next perturbation happens with the loss of load at the 120 s mark, the frequency error persists in the microgrid as seen in Fig. 6. This is because there is no change in the set-points of the DERs due to the absence of a centralized controller. Thus, once the centralized controller fails, the system will not perform satisfactorily.

On the other hand, the distributed scheme is able to ride through the loss of two control nodes at the 80 s and 100 s mark, respectively. Under the distributed scheme, when the microgrid loses load ℓ_6 at the 120 s mark, the remaining control nodes are able to act on the

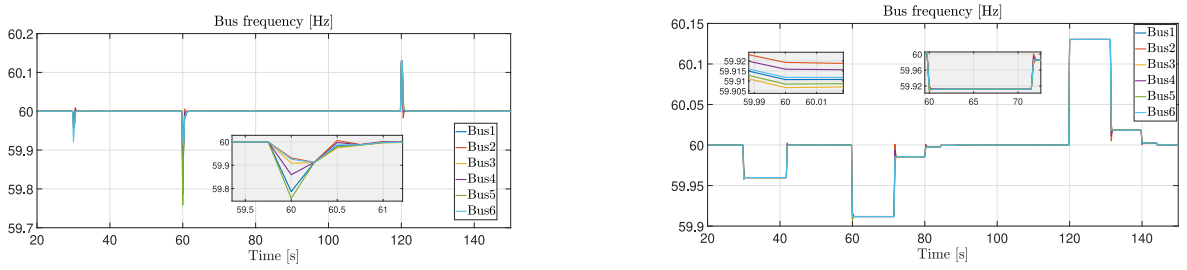

(a) Centralized secondary frequency control scheme.

(b) Distributed secondary frequency control scheme.

Fig. 4. Frequency response during implementation of both secondary frequency control schemes.

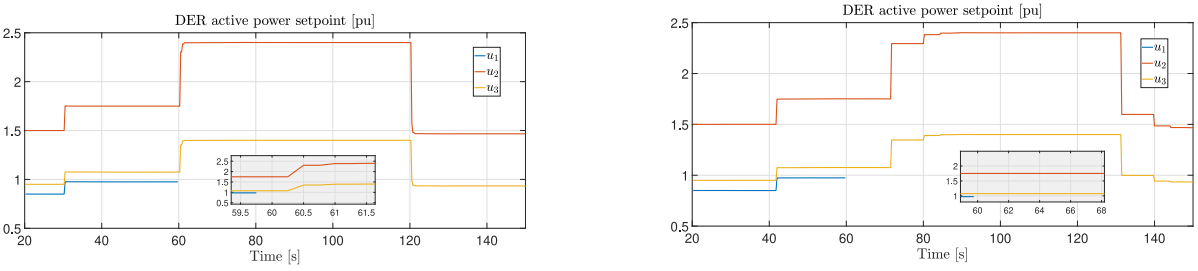

(a) Centralized secondary frequency control scheme.

(b) Distributed secondary frequency control scheme.

Fig. 5. Active power set-points of DERs during implementation of both secondary frequency control schemes.

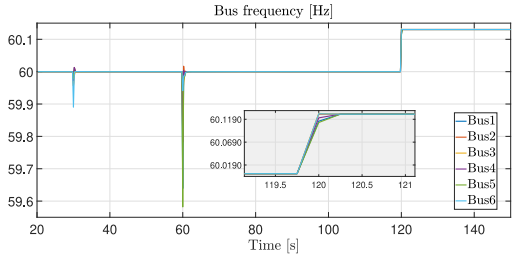

(a) Centralized secondary frequency control scheme.

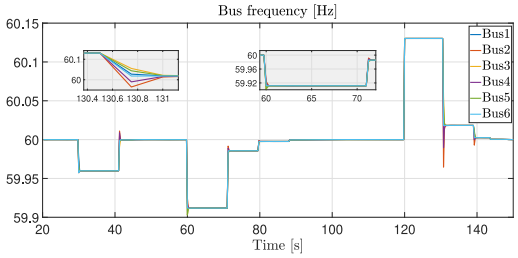

(b) Distributed secondary frequency control scheme.

Fig. 6. Frequency response during implementation of both control schemes under resilience test.

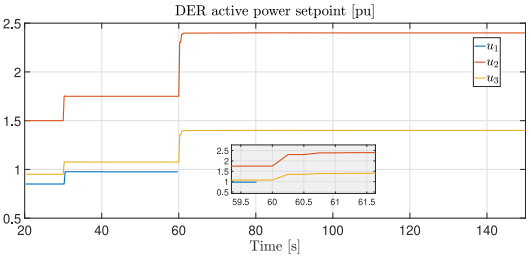

(a) Centralized secondary frequency control scheme.

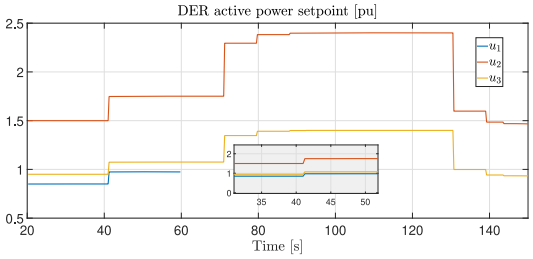

(b) Distributed secondary frequency control scheme.

Fig. 7. Active power set-points of DERs during implementation of both control schemes under resilience test.

perturbation and are able to bring the frequency back to 60 Hz. Under the loss of a control node, the system recovers and the remaining control nodes in the system work towards regulating frequency. Typically, under a loss of a control node, the distributed scheme takes more time to fix the frequency error and the additional time is due to the resilience protocol that the distributed scheme adopts.

5. Concluding remarks

In this paper, we provide a comparison of centralized vs. distributed schemes for microgrid secondary frequency control. We made use of two key performance objectives, namely response time and resilience, to identify the merits of the two schemes tested. We found that the response time of the centralized frequency control scheme is better than that of the distributed one. However, in terms of resilience, the distributed scheme outperforms the centralized scheme.

There is scope for improvements in terms of the response time when the distributed scheme loses control nodes. There are more performance objectives that we can use for benchmarking the distributed scheme such as scalability, cost of implementation (including operation and maintenance), and reliability. The experimental setup described can motivate future research to compare and benchmark other schemes for various microgrid control functions.

Declaration of Competing Interest

The authors declare that they have no known competing financial interests or personal relationships that could have appeared to influence the work reported in this paper.

References

[1] North American Electric Reliability Corporation, Distributed energy resources connection modeling and reliability considerations, Technical Report, (2017).
[2] A.D. Domínguez-García, C.N. Hadjicostis, N. Vaidya, Resilient networked control of distributed energy resources, IEEE J. Sel. Area. Comm. 30 (6) (2012) 1137–1148.
[3] D. Bakken, A. Bose, K.M. Chandy, P.P. Khargonekar, A. Kuh, S. Low, A. von Meier, K. Poolla, P.P. Varaiya, F. Wu, Grip - grids with intelligent periphery: Control architectures for grid2050$^{\alpha}$, Proc. of the IEEE International Conference on Smart Grid Communications, (2011), pp. 7–12.
[4] E. Mayhorn, L. Xie, K. Butler-Purry, Multi-time scale coordination of distributed energy resources in isolated power systems, IEEE Trans. Smart Grid 8 (2) (2017) 998–1005.
[5] R.H. Lasseter, Microgrids, Proc. of the Power Engineering Society Winter Meeting, 1 (2002), pp. 305–308 vol.1.
[6] F. Katiraei, M.R. Iravani, Power management strategies for a microgrid with multiple distributed generation units, IEEE Trans. Power Syst. 21 (4) (2006) 1821–1831, https://doi.org/10.1109/TPWRS.2006.879260.
[7] J.A.P. Lopes, C.L. Moreira, A.G. Madureira, Defining control strategies for microgrids islanded operation, IEEE Trans. Power Syst. 21 (2) (2006) 916–924, https://doi.org/10.1109/TPWRS.2006.873018.
[8] J.M. Guerrero, J.C. Vasquez, J. Matas, L.G. de Vicuna, M. Castilla, Hierarchical control of droop-controlled ac and dc microgrids—a general approach toward standardization, IEEE Trans. Ind. Electron. 58 (1) (2011) 158–172, https://doi.org/10.1109/TIE.2010.2066534.
[9] J.M. Guerrero, J.C. Vasquez, J. Matas, M. Castilla, L. Garcia de Vicuna, Control strategy for flexible microgrid based on parallel line-interactive ups systems, IEEE Trans. Ind. Electron. 56 (3) (2009) 726–736, https://doi.org/10.1109/TIE.2008.2009274.
[10] A.D. Domínguez-García, C.N. Hadjicostis, Distributed algorithms for control of demand response and distributed energy resources, Proc. of the IEEE Conference on Decision and Control, (2011), pp. 27–32.
[11] S.T. Cady, A.D. Domínguez-García, C.N. Hadjicostis, Robust implementation of distributed algorithms for control of distributed energy resources, Proc. of the North American Power Symposium, (2011), pp. 1–5.
[12] J.W. Simpson-Porco, F. Dörfler, F. Bullo, Synchronization and power sharing for droop-controlled inverters in islanded microgrids, Automatica 49 (9) (2013) 2603–2611, https://doi.org/10.1016/j.automatica.2013.05.018.
[13] S.T. Cady, A.D. Domínguez-García, C.N. Hadjicostis, A distributed generation control architecture for islanded ac microgrids, IEEE Trans. Control Syst. Technol. 23 (5) (2015) 1717–1735.
[14] R. Salcedo, E. Corbett, C. Smith, E. Limpaecher, R. Rekha, J. Nowocin, G. Lauss, E. Fonkwe, M. Almeida, P. Gartner, S. Manson, B. Nayak, I. Celanovic, C. Dufour, M.O. Faruque, K. Schoder, R. Brandl, P. Kotsampopoulos, T. Ham Ha, A. Davoudi, A. Dehkordi, K. Strunz, Banshee distribution network benchmark and prototyping platform for hardware-in-the-loop integration of microgrid and device controllers, J. Eng. 2019 (8) (2019) 5365–5373, https://doi.org/10.1049/joe.2018.5174.
[15] S.T. Cady, M. Zholbaryssov, A.D. Domínguez-García, C.N. Hadjicostis, A distributed frequency regulation architecture for islanded inertialess ac microgrids, IEEE Trans. Control Syst. Technol. 25 (6) (2017) 1961–1977.
[16] M. Chandorkar, D. Divan, R. Adapa, Control of parallel connected inverters in standalone ac supply systems, Ind. Appl. IEEE Trans. 29 (1) (1993) 136–143.

[17] K. De Brabandere, B. Bolsens, J. Van den Keybus, A. Woyte, J. Driesen, R. Belmans, A voltage and frequency droop control method for parallel inverters, Power Electron. IEEE Trans. 22 (4) (2007) 1107–1115.
[18] F. Dörfler, J.W. Simpson-Porco, F. Bullo, Breaking the hierarchy: distributed control and economic optimality in microgrids, IEEE Trans. Control Netw. Syst. 3 (3) (2016) 241–253, https://doi.org/10.1109/TCNS.2015.2459391.
[19] S.T. Cady, A.D. Domínguez-García, C.N. Hadjicostis, Finite-time approximate consensus and its application to distributed frequency regulation in islanded ac microgrids, Proc. of the Hawaii International Conference on System Sciences, (2015), pp. 2664–2670.
[20] C.N. Hadjicostis, N. Vaidya, A.D. Domínguez-García, Robust distributed average consensus via exchange of running sums, IEEE Trans. Automat. Contr. 61 (6) (2016) 1492–1507.
[21] O. Azofeifa, S. Nigam, O. Ajala, C. Sain, S. Utomi, A.D. Domínguez-García, P.W. Sauer, Controller hardware-in-the-loop testbed for distributed coordination and control architectures, Proc. of North American Power Symposium, Wichita, KS, (2019).